THE JOURNAL OF PHYSICAL CHEMISTRY C

Article

Cite This: J. Phys. Chem. C 2019, 123, 5061−5066

pubs.acs.org/JPCC

Polychromatic Photoluminescence of Polymorph Boron Dipyrromethene Crystals and Heterostructures

Aswin Asaithambi,[†,#] Daichi Okada,[‡,#] Günther Prinz,[†] Hiroyasu Sato,[§] Akinori Saeki,[∥] Takashi Nakamura,[⊥] Tatsuya Nabeshima,[⊥] Yohei Yamamoto,[‡] and Axel Lorke*[,†]

[†]Faculty of Physics and CENIDE, University of Duisburg-Essen, Lotharstr. 1, Duisburg 47057, Germany

[‡]Division of Materials Science, Faculty of Pure and Applied Sciences, University of Tsukuba, 1-1-1 Tennodai, Tsukuba, Ibaraki 305-8573, Japan

[§]Rigaku Corporation, Akishima, Tokyo 196-8666, Japan

[∥]Department of Applied Chemistry, Graduate School of Engineering, Osaka University, 2-1 Yamadaoka, Suita, Osaka 565-0871, Japan

[⊥]Division of Chemistry, Faculty of Pure and Applied Sciences, University of Tsukuba, 1-1-1 Tennodai, Tsukuba, Ibaraki 305-8577, Japan

Supporting Information

ABSTRACT: Micrometer-sized boron dipyrromethene crystalline rods were grown from solution. Fluorescence microscopy images reveal that each rod displays characteristic visible light emission of a different color. In a particular case, optical heterostructures with discrete, differently colored sections are observed within a single microrod. Microphotoluminescence (μ-PL) spectra of green and red rods at room temperature show multiple contributions, indicating the presence of microdomains. Temperature-dependent μ-PL measurements further confirm this, as red emission decreases and green emission increases at lower temperatures. These observations are discussed as a result of crystalline polymorphism, leading to a local variation of the highest occupied molecular orbital−lowest unoccupied molecular orbital energy difference. An Arrhenius plot quantifies the hopping barrier for the charge carriers to reach the low emission energy (red) regions. A line scan of a single rod further supports that microdomains of green- and orange−red-emitting crystal phases are present in a single rod. Time-resolved microwave conductivity studies clarify that microdomain-free green rods display 2 orders of magnitude longer photocarrier lifetime and 5-fold higher photoconductivity than the red rods with many small band-gap regions.

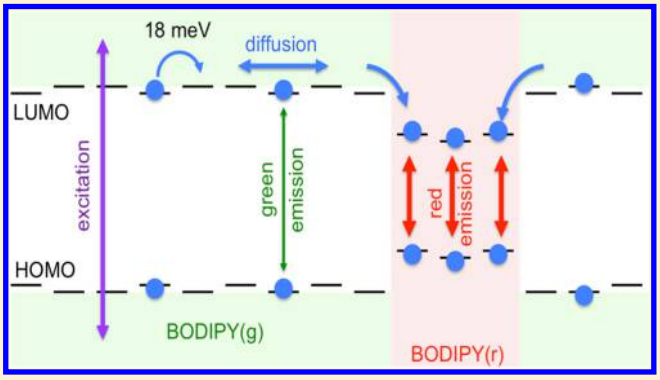

INTRODUCTION

Boron dipyrromethene (BODIPY) dyes are a class of optically active organic compounds, based on a 4,4-difluoro-4-bora-3a,4a-diaza-s-indacene (or boron dipyrromethene) core.[1,2] Because of their high fluorescence quantum yield and tunable emission wavelength, they have found a wide range of applications, e.g., as fluorescent labels, chemical sensors, or laser dyes.[3−5] They exhibit long-term stability and are compatible with polymer technologies, which makes them attractive for use in solar cell concentrators[6] and organic light-emitting devices.[7] Variations to their structure make it possible to tune their optical properties and solubility.[8]

For technical applications, the solid form of BODIPY is more desirable than its solution.[6] In the crystal form, however, interaction among the molecules, such as J or H aggregation, may lead to blue- or red-shifted emission. Aggregation can even lead to a complete quenching of the fluorescence.[9] One strategy to overcome this problem is the introduction of a suitable group at the meso position to prevent aggregation through steric hindrance.[10]

Here, we investigate the optical properties of microcrystals of the BODIPY derivative shown in Figure 1a.[11] A 5 mM solution of BODIPY in tetrahydrofuran (THF) is injected into water with cetrimonium bromide (CTAB) as a surfactant, and the mixture is sonicated for 5 min. Allowing the solution to settle overnight leads to the formation of micrometer-sized rods with a crystalline habit (see Figure 1b). Note that the presence of the surfactant improves crystal growth; however, it does not affect the optical properties of the resulting microrods, discussed below. Also, THF can be replaced by acetone or ethanol without changing the results (see Figures S1 and S2).

Received: September 20, 2018
Revised: October 30, 2018
Published: November 2, 2018

DOI: 10.1021/acs.jpcc.8b09202
J. Phys. Chem. C 2019, 123, 5061−5066

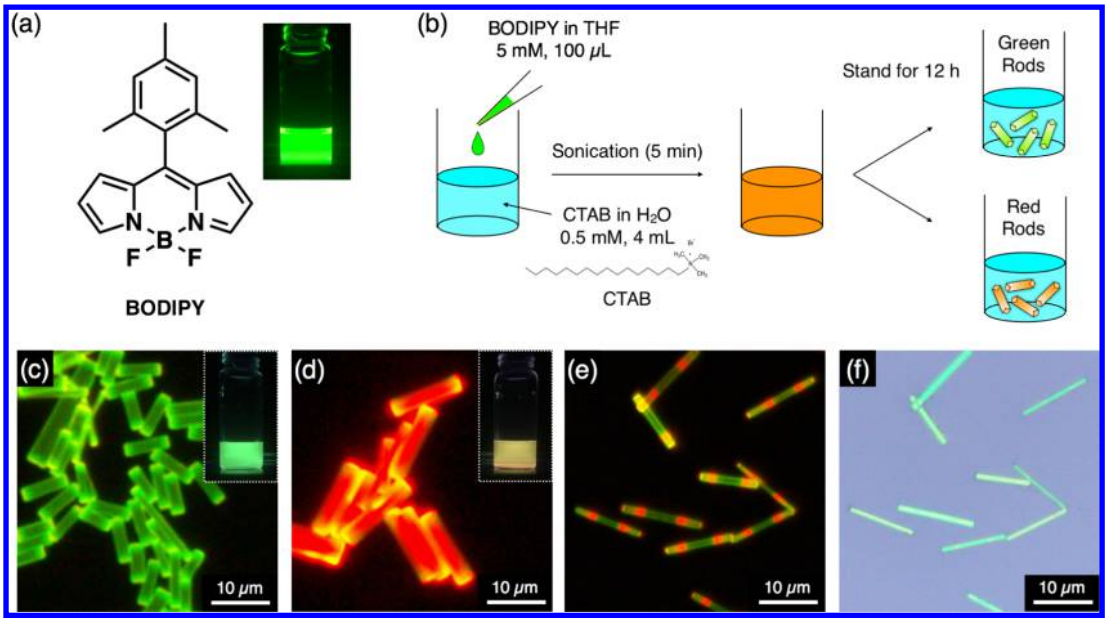

Figure 1. (a) Molecular structure of BODIPY and its fluorescence in THF solution (excitation wavelength λ_{ex} = 365 nm). (b) Schematic representation of the preparation procedures of green and red rods of BODIPY. Fluorescence microscopy images of (c) green and (d) red BODIPY rods; λ_{ex} = 400−450 nm. The bright spots at the end of the rods indicate light guidance by total internal reflection[2] and demonstrate the high optical quality of the microcrystals. The insets in (c) and (d) show the appearance of the microcrystals in solution under UV illumination. (e) Fluorescence and (f) optical microscopy images of BODIPY rods with an optical heterostructure; λ_{ex} = 400−450 nm.

RESULTS AND DISCUSSION

Figure 1c,d shows fluorescence microscopy images of typical microrods, fabricated as described above. Under near-ultraviolet illumination (400−450 nm wavelength), the rods exhibit bright green light emission, similar to the emission from BODIPY in THF, shown in the inset of Figure 1a. While green-emitting rods are the most common, we also find rods with different colors, ranging from green all the way to red (see Figure 1d). Using the described fabrication method, the resulting color of the rods is not well defined; we observe microcrystals with different emissions in different batches (see Figures 1c,d, S1, and S2) and even single rods with discrete, differently colored sections (see Figure 1e). At room temperature, the fluorescence quantum yields are 0.12 and 0.10 for the green and red rods, respectively.

While in the present study, we focus on a specific compound, we would like to point out that these findings are more general in their scope. For example, Spies et al. have made similar observations on a different BODIPY derivative.[12] They were able to obtain different crystal habits, depending on the details of the crystallization process, and found that different crystal habits exhibited different emission colors. Because all habits had the same short-range order crystalline structure, the authors concluded that a very long-range order is crucial for the optical properties of the investigated BODIPY crystal. We propose that the different emission colors, observed in the present study, have the same origin.

To better quantify the emission characteristics of the present crystals, we performed microphotoluminescence (μ-PL) spectroscopy on single rods. PL spectra under 405 nm laser light excitation for "green" and "red" rods are given in Figure 2a,b, respectively. As expected, the green rod exhibits strong emission around 550 nm, while the red rod mainly emits in the region above 650 nm. Note, however, that both rods show light emission over the entire spectral range between 525 and ≈800 nm. The distinct, short wavelength cutoff at 525 nm in

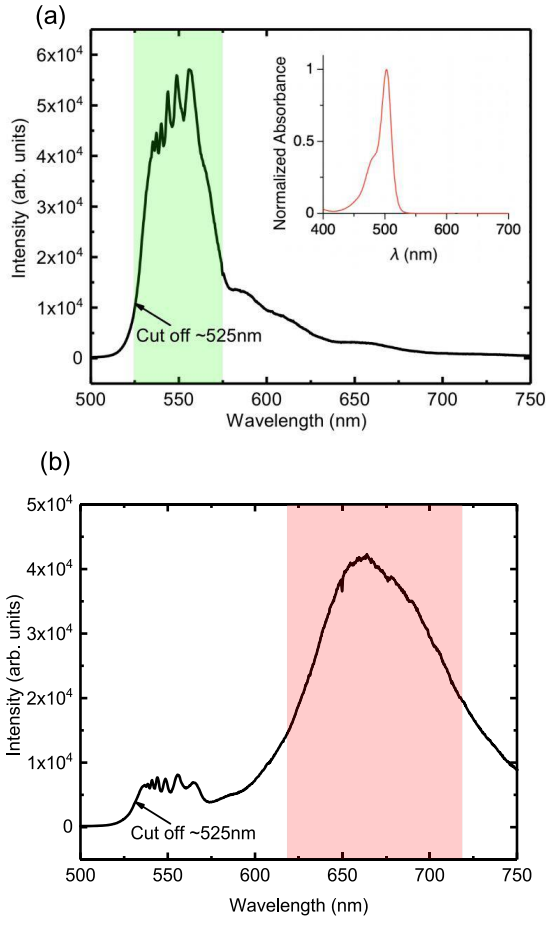

Figure 2. PL spectra of (a) green-emitting and (b) red-emitting BODIPY rods at 296 K. The inset in (a) shows the absorption spectrum of the BODIPY monomer in solution.

DOI: 10.1021/acs.jpcc.8b09202
J. Phys. Chem. C 2019, 123, 5061−5066

both spectra agrees well with the absorption edge of the BODIPY monomer in solution, shown in the inset of Figure 2a.

These observations lead us to conclude that there are different species present in the rods, which emit in different spectral regions (green, orange, or red). The colors that appear in the fluorescence microscopy images are the result of different amounts of the respective species in each rod. Even rods that do not have as well-separated phases as the ones in Figure 1e but seem macroscopically homogeneous are composed of domains with different emission properties.

This assumption is supported by temperature-dependent PL spectroscopy on a single rod. Figure 3 shows how the PL of a red rod evolves, as the temperature T is lowered from 296 to 85 K. With decreasing T, the emission in the red (around 650 nm) decreases, while at the same time, the green part of the spectrum increases in intensity. Note that the individual peaks in the spectrum do not shift but rather change their relative intensities. As an example, the dominant peak in the low-temperature spectrum is indicated by an arrow in the high-temperature data. PL measurements of green rods, on the other hand, do not show such a pronounced temperature-dependent change in the spectral weights (see Figure S4). Furthermore, at low temperatures, the PL spectra of green and red rods become quite similar.

In the following, we explain these experimental observations using a simple model, on the basis of the fact that the solid form of BODIPY can exist in different crystal modifications. Such polymorphism in BODIPY was first reported by Luo et al.[13] For 4-methoxycarbonylphenyl-substituted BODIPY, they found several different crystalline polymorphs, which exhibit characteristically different emission properties. For the present compound, we assume that at least two crystalline polymorphs can be present in a single rod. One of them (labeled BODIPY(g) in the following) has a large highest occupied molecular orbital−lowest unoccupied molecular orbital (HOMO−LUMO) separation, characterized by PL emission in the range of 530−580 nm, similar to that of the BODIPY monomer, but somewhat red-shifted because of its crystalline order. The other modification, BODIPY(r), exhibits a reduced HOMO−LUMO energy difference, and hence emission in the red spectral range, possibly caused by the coupling of molecular orbitals among neighboring molecules. Figure 4 schematically depicts the resulting energy landscape when a small amount of BODIPY(r) is embedded in BODIPY(g).

At room temperature, electron−hole pairs that are optically excited in BODIPY(g) can diffuse to the regions with BODIPY(r), where they recombine by the emission of red light. Therefore, even in rods that predominantly consist of BODIPY(g), the PL emission will appear as red. This somewhat resembles the processes in inorganic semiconductor heterostructures, such as GaAs/AlGaAs quantum wells, where the PL emission also will be dominated by recombination in the low-band-gap region (GaAs), even when the material is excited in the high-band-gap environment (AlGaAs).[14] Note that, comparing Figure 1e,f, the optical microscopy images do not show a clear stripe pattern, indicating that photoabsorption is almost identical for both BODIPY(g) and BODIPY(r), which supports the model shown in Figure 4.

With decreasing temperature, diffusion of the optically generated carriers will be reduced, and fewer of them will be able to reach the low-energy regions of BODIPY(r). Therefore, the red emission will decrease in intensity, while the green emission will increase (see Figure 3a). Figure 3b quantifies the thermally induced diffusion by an Arrhenius plot of the ratio of the green (560 nm) and red (650 nm) emission intensities. The fit (red line) gives an activation energy of 18 meV, which

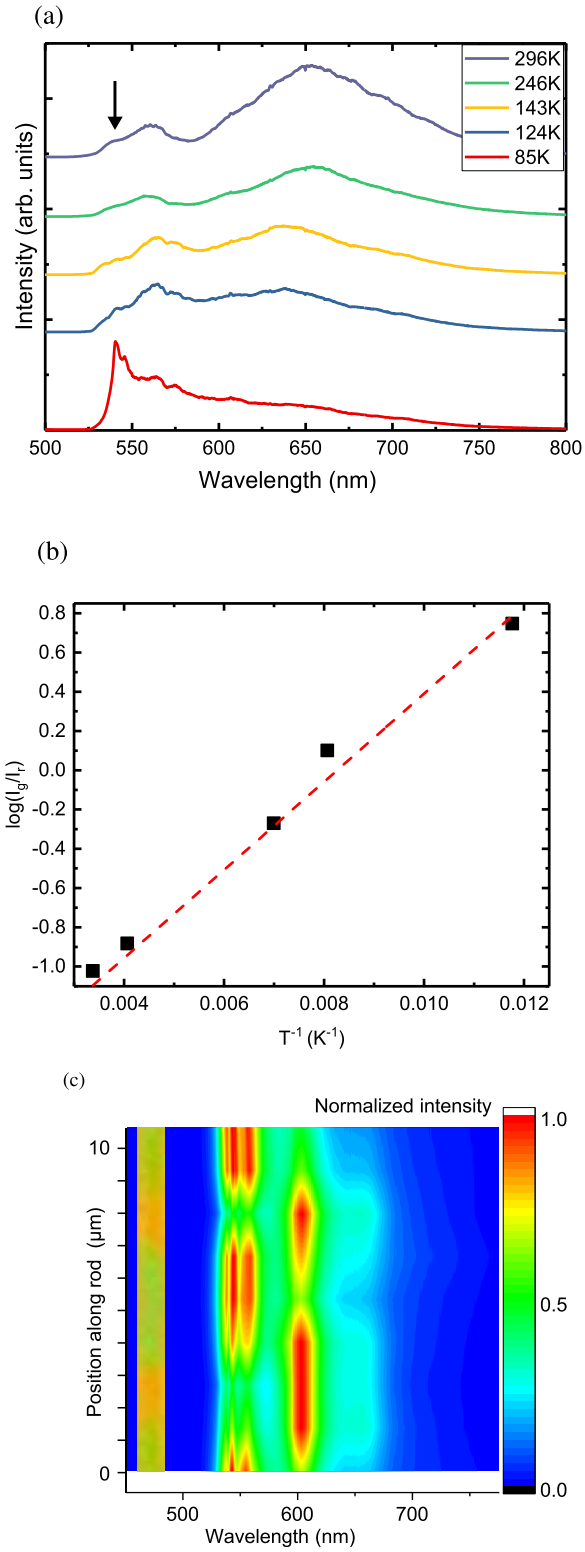

Figure 3. (a) PL spectra of a red-emitting BODIPY rod at different temperatures. (b) Arrhenius plot of the ratio between green and red intensities at different temperatures. (c) Room temperature line scan along a single, striped BODIPY rod, shown on the left (color enhanced).

DOI: 10.1021/acs.jpcc.8b09202
J. Phys. Chem. C 2019, 123, 5061−5066

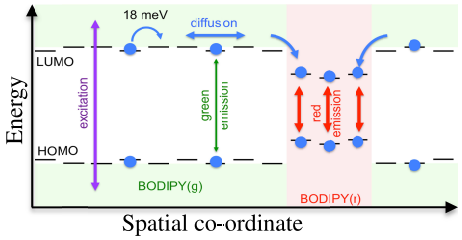

Figure 4. Model showing the energy landscape in real space of a single rod that describes the hopping and recombination of excited charge carriers in different regions (BODIPY(g) and BODIPY(r)).

we identify as a typical hopping barrier within BODIPY(g), as indicated in Figure 4.

Depending on the amount of regions composed of BODIPY(r), the intensity ratio between the green and the red emission bands will vary along a single well-shaped rod if the ratio between BODIPY(g) and BODIPY(r) is changing. This was indeed observed for line scans of the emission at room temperature along single, striped rods (see Figure 3c), which corroborates the model given above that small regions (presumably below 1 μm) of BODIPY(r) are incorporated in BODIPY(g).

Flash-photolysis time-resolved microwave conductivity (FP-TRMC) experiments clearly show the difference of photogenerated charge carrier half-life ($\tau_{1/2}$) and $\phi\sum\mu$ (the product of the photon-to-carrier conversion efficiency and the sum of charge carrier mobilities) between BODIPY(g) and BODIPY(r) (Figure 5a).[15] The $\tau_{1/2}$ value of BODIPY(g) is 7.7×10^{-5} s, which is roughly 2 orders of magnitude longer than that of BODIPY(r) (8.9×10^{-7} s, Figure 5b). Furthermore, $\phi\sum\mu$ of BODIPY(g) (2.8×10^{-4} cm^2 V^{-1} s^{-1}) is ~5-fold greater than that of BODIPY(r) (5.5×10^{-5} cm^2 V^{-1} s^{-1}, Figure 5c). These results support the assumption that microcrystals of BODIPY(r) have many narrow band-gap sites, which trap photocarriers efficiently after the laser flash, leading to shorter $\tau_{1/2}$ and smaller $\phi\sum\mu$ in comparison with those of almost trap-free BODIPY(g) microrods. Taking $\phi\sum\mu \approx 3 \times 10^{-4}$ cm^2 V^{-1} s^{-1} as a lower limit for the carrier mobility and using the Einstein relation, we can estimate the diffusion constant in the green rods, $D \approx 8 \times 10^{-10}$ m^2 s^{-1}. Together with the measured carrier lifetime $\tau_{1/2} \approx 10^{-4}$ s, this gives a rough estimate of around 1 μm for the diffusion length (see the Supporting Information). Therefore, diffusion of photoexcited carriers can cover large areas inside the rods until they encounter a recombination site, as depicted in Figure 4.

We were able to obtain a single crystal of BODIPY(r) with a dimension of $0.41 \times 0.058 \times 0.013$ mm^3, which is large enough for single-crystal X-ray diffraction (XRD) studies. According to the XRD data, BODIPY(r) forms orthorhombic crystals with space group *Pbca* (see the Supporting Information, Figure S4 and Table S1). Importantly, the crystal structure hardly changes upon cooling from 298 K (red PL) to 93 K (green PL) with only less than 1.5% shrinking of the lattice parameter. These results indicate that the change of the PL color upon lowering T does not result from the structural phase transition but from the change of the diffusion length of photogenerated charge carriers, as proposed in Figure 4. The crystal packing of the BODIPY molecules (Figure S4) is incompatible with J or H aggregation; therefore, the green and orange emission energies cannot be explained by aggregation-induced, bathochromic or hypsochromic shifts with respect to the monomer.

Unfortunately, a single crystal of BODIPY(g), large enough for XRD, has not been obtained. However, the powder XRD pattern of BODIPY(g) is almost identical to that of BODIPY(r) (Figure S5). Small differences in the relative intensities of the peaks and additional structure at low scattering angles (<10°) may indicate, however, different long-range orders in BODIPY(g) and BODIPY(r).

The co-existence of two crystal phases with different optical properties has also been recently observed in the solution-mediated growth of GaAs nanowires.[16] While GaAs will generally crystallize in the zincblende structure, the high liquid supersaturation present in the growth of gold-catalyzed GaAs nanowires can lead to the formation of wurtzite GaAs.[16−18] This follows the Ostwald step rule,[19] which states that rapid crystallization from a solution takes place so that a thermodynamically unstable phase occurs first, which then, in a second step, will recrystallize into a more stable phase. We believe that a similar mechanism is at work in the present compound, with BODIPY(g) being the less stable modification and BODIPY(r) the more stable one. Indeed, we find that rapid growth will preferentially result in green-emitting rods, while slow growth will lead to more red-emitting crystals. Also, green-emitting rods that are exposed to ethanol vapor for extended periods (12−36 h of solvent annealing[20]) will slowly convert to red-emitting ones (Figure 6).

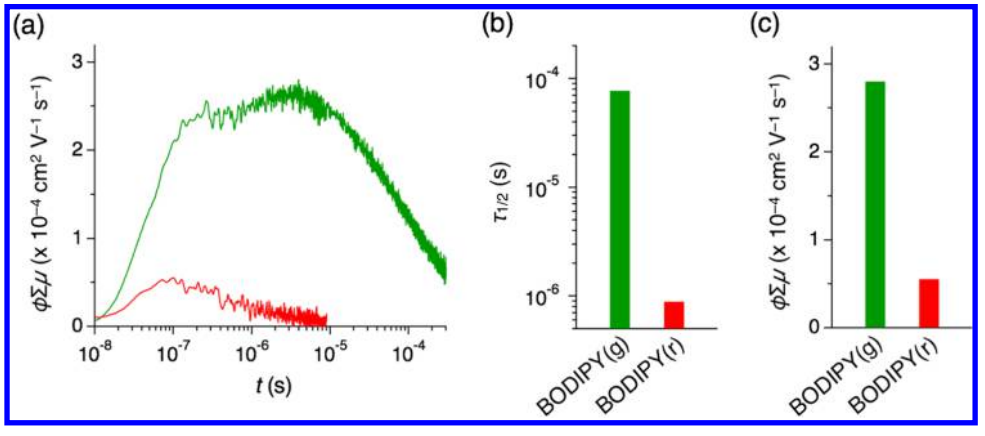

Figure 5. (a) TRMC profiles at 25 °C of cast films of BODIPY(g) (green) and BODIPY(r) (red) upon a laser flash at 355 nm. Bar graphs of (b) $\tau_{1/2}$ and (c) $\phi\sum\mu$ for BODIPY(g) (green) and BODIPY(r) (red).

DOI: 10.1021/acs.jpcc.8b09202
J. Phys. Chem. C 2019, 123, 5061−5066

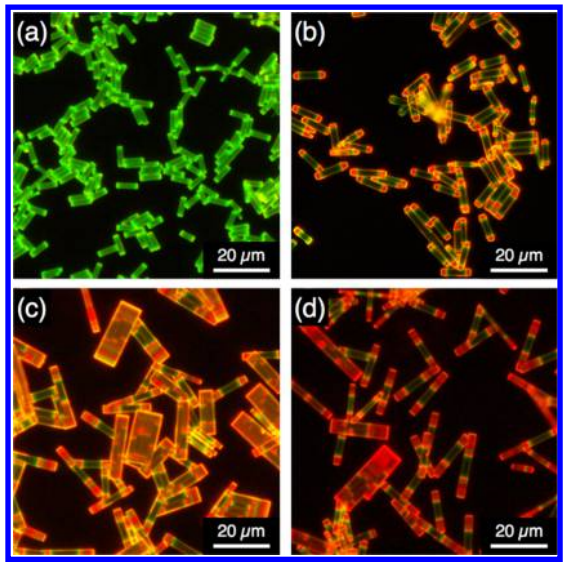

Figure 6. Fluorescence micrograph of initially green BODIPY rods (a) before and after exposure to EtOH vapor for (b) 12, (c) 24, and (d) 36 h.

While this demonstrates some degree of control over the emission properties of the rods, (BODIPY(g) vs BODIPY(r)), it would be highly desirable to find growth conditions that enable a precise control over the stepwise variation in the HOMO−LUMO gap (similar to the serendipitously created, striped crystals in Figure 1e,f). This would open up the possibility to tailor the energy landscape in a similar fashion as the "bandstructure engineering" in inorganic binary and ternary semiconductor compounds.[14]

Finally, we would like to briefly mention a set of resonances that appear near the emission edge in the green part of the spectrum (e.g., in the range of 530−560 nm in Figure 2a). The nature of these peaks is not fully understood so far. However, the fact that they can be very well described by a Wannier series, $E_n = E_g - E^*_{RY}/n^2$, rules out Fabry−Pérot-type optical resonances and strongly suggests an excitonic origin. Here, E_n is the energy of the nth resonance, E_g the emission cutoff energy or band gap (corresponding to a wavelength of 525 nm), and E^*_{RY} the effective Rydberg energy. More detailed studies will be necessary to elucidate this phenomenon.

CONCLUSIONS

In summary, micrometer-sized crystalline rods of BODIPY were grown from solution. Fluorescence microscopy images and photoluminescence spectra show different forms of BODIPY, emitting in the green, orange, and red spectral regions. From temperature-dependent photoluminescence, it is concluded that BODIPY crystals can exhibit different HOMO−LUMO gaps, and optically excited carriers can diffuse from the wide-gap to the narrow-gap region with a typical hopping barrier of ≈18 meV. This model is supported by PL line scans along striped rods and by FP-TRMC. Different growth rates and solvent annealing suggest that the orange−red-emitting crystal structure is a thermodynamically more stable form of BODIPY. These findings may lead to optically active BODIPY heterostructures, similar to those used in inorganic semiconductor technology.

EXPERIMENTAL METHODS

Unless otherwise noted, reagents and solvents were used as received from Sigma-Aldrich Chemical Co. Ltd and Nakarai Tesque Co., respectively. BODIPY was synthesized according to the reported procedures.[2] Scanning electron microscopy (SEM) was performed at 25 °C on a Hitachi model S-4800 FE-SEM and JEOL model JSM-5610 SEM operating at 10 and 20 kV, respectively. Silicon was used as a substrate and Pt or Au for coating. Powder X-ray diffraction patterns were recorded at 298 K on a Rigaku model MultiFlex X-ray diffractometer with a Cu Kα radiation source. Fluorescence spectra were recorded at 25 °C with a JASCO model FP-6200 spectrofluorometer. Electronic photoabsorption and diffuse reflectance spectra were recorded at 25 °C with a JASCO model V-570 UV/vis/NIR spectrophotometer equipped with an ISN-470 integrating sphere accessory for the diffuse reflectance spectroscopy. Flash-photolysis time-resolved microwave conductivity (FP-TRMC) measurements were carried out at 25 °C in air, where the resonant frequency and microwave power were set at ∼9.1 GHz and 3 mW, respectively, so that the electric field of the microwave was small enough not to disturb the thermal motion of charge carriers.[15] The charge carriers were photochemically generated using the third-harmonic generation (355 nm) light pulses from a Continuum model Surelite II Nd:YAG laser (5−8 ns pulse duration) with incident photon densities of 9.1×10^{15} photons cm^{-2}. The TRMC signals, picked up by a diode (rise time < 1 ns), were monitored by a Tektronics model DPO4104 digital oscilloscope. The observed conductivities were converted into normalized values, given by a photocarrier generation yield (ϕ) multiplied by the sum of the charge carrier mobilities ($\sum\mu$), according to an equation $\phi\sum\mu = (1/eAI_0F_{light})(\Delta P_r/P_r)$, where e, A, I_0, F_{light}, P_r, and ΔP_r denote the unit charge of a single electron, the sensitivity factor (S^{-1} cm), the incident photon density of an excitation laser (photon cm^{-2}), the filling factor (cm^{-1}), and the reflected microwave power and its change, respectively. Microphotoluminescence measurements were performed using a custom-built setup, which allows us to take images of the rods, when exciting with a white light source, or to record the emission spectra when exciting with a 405 nm laser. The exciting light is focused on the sample with a 50× microscope objective, leading to a laser spot size of ∼1 μm. The emitted light is then collected by the same objective and dispersed in an Acton 2500i spectrometer with an attached liquid-nitrogen-cooled Princeton Research CCD camera. For the temperature-dependent emission measurements, we used a continuous-flow liquid helium cryostat (Janis Inc.).

ASSOCIATED CONTENT

Supporting Information

The Supporting Information is available free of charge on the ACS Publications website at DOI: 10.1021/acs.jpcc.8b09202.

Photoluminescence (PL) spectra of BODIPY rods without CTAB, fluorescence microscopy images showing the effect of solvent annealing, temperature-dependent PL spectra of BODIPY(g), crystallography information about BODIPY(g) and BODIPY(r), and scanning electron microscopy images of striped BODIPY rods (PDF)

DOI: 10.1021/acs.jpcc.8b09202
J. Phys. Chem. C 2019, 123, 5061−5066

AUTHOR INFORMATION

Corresponding Author

*E-mail: axel.lorke@uni-due.de.

ORCID

Akinori Saeki: 0000-0001-7429-2200
Takashi Nakamura: 0000-0002-1864-1143
Tatsuya Nabeshima: 0000-0003-1269-7725
Yohei Yamamoto: 0000-0002-2166-3730
Axel Lorke: 0000-0002-0405-7720

Author Contributions

#A.A. and D.O. contributed equally to this work.

Notes

The authors declare no competing financial interest.

ACKNOWLEDGMENTS

This work was supported by a Grant-in-Aid for Scientific Research on Innovative Areas "π-System Figuration" (JP17H05142), Scientific Research (A) (JP16H02081) from the Japan Society for the Promotion of Science (JSPS), University of Tsukuba Pre-strategic Initiative "Ensemble of light with matters and life", TIA Kakehashi, and Asahi Glass Foundation. A.A. thanks IMPRS-SurMat for the doctoral fellowship.

REFERENCES

(1) Burghart, A.; Kim, H.; Welch, M. B.; Thoresen, L. H.; Reibenspies, J.; Burgess, K.; Bergström, F.; Johansson, L. B. 3,5-Diaryl-4,4-difluoro-4-bora-3a,4a-diaza-s-indacene (BODIPY) Dyes: Synthesis, Spectroscopic, Electrochemical, and Structural Properties. *J. Org. Chem.* **1999**, *64*, 7813−7819.

(2) Okada, D.; Nakamura, T.; Braam, D.; Dao, T. D.; Ishii, S.; Nagao, T.; Lorke, A.; Nabeshima, T.; Yamamoto, Y. Color-Tunable Resonant Photoluminescence and Cavity-Mediated Multistep Energy Transfer Cascade. *ACS Nano* **2016**, *10*, 7058−7063.

(3) Ehrenschwender, T.; Wagenknecht, H.-A. 4,4-Difluoro-4-bora-3a,4a-diaza-s-indacene as a Bright Fluorescent Label for DNA. *J. Org. Chem.* **2011**, *76*, 2301−2304.

(4) Monsma, F. J., Jr.; Barton, A. C.; Kang, H. C.; Brassard, D. L.; Haughland, R. P.; Sibley, D. R. Characterization of Novel Fluorescent Ligands with High Affinity for D1 and D2 Dopaminergic Receptors. *J. Neurochem.* **1989**, *52*, 1641−1644.

(5) Shah, M.; Thangraj, K.; Soong, M. L.; Wolford, L.; Boyer, J. H.; Politzer, I. R.; Pavlopoulos, T. G. Pyrromethene-BF2 Complexes as Laser Dyes:1. *Heteroat. Chem.* **1990**, *1*, 389−399.

(6) Bozdemir, O. A.; Erbas-Cakmak, S.; Ekiz, O. O.; Dana, A.; Akkaya, E. U. Towards unimolecular luminescent solar concentrators: bodipy-based dendritic energy-transfer cascade with panchromatic absorption and monochromatized emission. *Angew. Chem., Int. Ed.* **2011**, *50*, 10907−10912.

(7) Tang, C. W.; VansSlyke, S. A. Organic electroluminescent diodes. *Appl. Phys. Lett.* **1987**, *51*, 913.

(8) Xiao, S.; Zou, Y.; Wu, J.; Zhou, Y.; Yi, T.; Li, F.; Huang, C. Hydrogen Bonding Assisted Switchable Fluorescence in Self-Assembled Complexes Containing Diarylethene: Controllable Fluorescent Emission in the Solid State. *J. Mater. Chem.* **2007**, *17*, 2483−2489.

(9) Kim, H. S.; Park, S.-R.; Suh, M. C. Concentration Quenching Behavior of Thermally Activated Delayed Fluorescence in a Solid Film. *J. Phys. Chem. C* **2017**, *121*, 13986−13997.

(10) Ozdemir, T.; Atilgan, S.; Kutuk, I.; Yildirim, L. T.; Tulek, A.; Bayindir, M.; Akkaya, E. U. Solid-State Emissive BODIPY Dyes with Bulky Substituents As Spacers. *Org. Lett.* **2009**, *11*, 2105−2107.

(11) Kee, H. L.; Kirmaier, C.; Yu, L.; Thamyongkit, P.; Youngblood, W. J.; Calder, M. E.; Ramos, L.; Noll, B. C.; Bocian, D. F.; Scheidt, W. R.; Birge, R. R.; Lindsey, J. S.; Holten, D. Structural Control of the Photodynamics of Boron-Dipyrrin Complexes. *J. Phys. Chem. B* **2005**, *109*, 20433−20443.

(12) Spies, C.; Huynh, A.-M.; Huch, V.; Jung, G. Correlation between Crystal Habit and Luminescence Properties of 4,4-Difluoro-1,3-dimethyl-4-bora-3a,4a-diaza-s-indacene, An Asymmetric BODIPY Dye. *J. Phys. Chem. C* **2013**, *117*, 18163−18169.

(13) Luo, G.-G.; Xia, J.-X.; Fang, K.; Zhao, Q.-H.; Wu, J.-H.; Dai, J.-C. Discovery of polymorphism-dependent emission for crystalline boron-dipyrromethene dye. *Dalton Trans.* **2013**, *42*, 16268−16271.

(14) Fox, M.; Ispasoiu, R. Quantum Wells, Superlattices, and Band-Gap Engineering. In *Springer Handbook of Electronic and Photonic Materials*; Kasap, S., Capper, P., Eds.; Springer: Cham, 2017.

(15) Saeki, A.; Yamamoto, Y.; Koizumi, Y.; Fukushima, T.; Aida, T.; Seki, S. Photoconductivity of Self-Assembled Hexabenzocoronene Nanotube: Insight into the Charge Carrier Mobilities on Local and Long-Range Scales. *J. Phys. Chem. Lett.* **2011**, *2*, 2549−2554.

(16) Spirkoska, D.; Arbiol, J.; Gustafsson, A.; Conesa-Boj, S.; Glas, F.; Zardo, I.; Heigoldt, M.; Gass, M. H.; Bleloch, A. L.; Estrade, S.; Kaniber, M.; Rossler, J.; Peiro, F.; Morante, J. R.; Abstreiter, G.; Samuelson, L.; Fontcuberta i Morral, A. Structural and optical properties of high quality zinc-blende/wurtzite GaAs nanowire heterostructures. *Phys. Rev. B* **2009**, *80*, No. 245325.

(17) Glas, F.; Harmand, J.-C.; Patriarche, G. Why Does Wurtzite Form in Nanowires of III-V Zinc Blende Semiconductors? *Phys. Rev. Lett.* **2007**, *99*, 146101−146104.

(18) Joyce, H. J.; Wong-Leung, J.; Gao, Q.; Hoe Tan, H.; Jagadish, C. Phase Perfection in Zinc Blende and Wurtzite III−V Nanowires Using Basic Growth Parameters. *Nano Lett.* **2010**, *10*, 908−915.

(19) Van Santen, R. A. The Ostwald step rule. *J. Phys. Chem.* **1984**, *88*, 5768−5769.

(20) Sinturel, C.; Vayer, M.; Morris, M.; Hillmyer, M. A. Solvent Vapor Annealing of Block Polymer Thin Films. *Macromolecules* **2013**, *46*, 5399−5415.

DOI: 10.1021/acs.jpcc.8b09202
J. Phys. Chem. C 2019, 123, 5061−5066